Journal of Pathology
J Pathol 2019; **248:** 155–163
Published online 20 February 2019 in Wiley Online Library (wileyonlinelibrary.com) DOI: 10.1002/path.5240

ORIGINAL PAPER

Hepatitis C virus infection induces endoplasmic reticulum stress and apoptosis in human fetal liver stem cells

Xuan Guo[1,2,3], Wei-Li Liu[1], Dong Yang[1], Zhi-Qiang Shen[1], Zhi-Gang Qiu[1], Min Jin[1]* and Jun-Wen Li[1]*

[1] *Tianjin Institute of Environmental and Operational Medicine, Tianjin, PR China*
[2] *Research Institute of Chemical Defense, Beijing, PR China*
[3] *State Key Laboratory of NBC Protection for Civilian, Beijing, PR China*

**Correspondence to: J-W Li or M Jin, Tianjin Institute of Environmental and Operational Medicine, No. 1 Dali Road, Tianjin 300050, PR China. E-mail: junwen9999@hotmail.com or jinminzh@126.com*

Abstract

The cellular mechanisms by which hepatitis C virus (HCV) replication might mediate cytopathic effects are controversial and not entirely clear. In this study, we found that blood-borne HCV (bbHCV) infection could lead to endoplasmic reticulum (ER)-stress and mitochondria-related/caspase-dependent apoptosis at the early stages of infection based on use of the highly efficient bbHCV cell culture model established previously. Sections of bbHCV-infected human fetal liver stem cells (hFLSCs) revealed convolution and nonlinear ER, cell vacuolization, swelling of mitochondria, and numerous double membrane vesicles (DMVs). The percentage of apoptotic hFLSCs infected by bbHCV reached 29.8% at 16 h postinfection, and the amount of cytochrome c increased remarkably in the cytosolic protein fraction. However, over time, apoptosis was inhibited due to the activation of NF-κB. The expression of NF-κB-p65, Bcl-xL, XIAP, and c-FLIPL in hFLSCs was increased significantly 24 h after in infection by bbHCV. The accelerated cell death cycles involving apoptosis, regeneration and repair by bbHCV infection might give rise to the development of cirrhosis, and ultimately to hepatocellular carcinogenesis.

Keywords: human fetal liver stem cells; hepatitis C virus infection; cytopathic effect; apoptosis

Received 6 October 2018; Revised 29 November 2018; Accepted 16 January 2019

No conflicts of interest were declared.

Introduction

With 200 million people infected worldwide, hepatitis C virus (HCV) has become a global health problem and a major cause of viral hepatitis. Persistent infection occurs in 70% of infected patients followed by some serious complications such as inflammation, insulin resistance, steatosis, fibrosis, and hepatocellular carcinoma. The pathology associated with chronic HCV infection was initially thought to be related with HCV-specific immune responses [1,2]. But now there are some who view that direct cytopathic effects (CPEs) in virally infected cells also contribute substantially to HCV-associated liver injury [3,4]. The cellular mechanisms by which HCV replication might mediate liver injury are not entirely clear. Sekine-Osajima *et al* investigated the cellular effects of HCV infection and replication using the HCV-JFH1 cell culture system and found that HCV-JFH1 infected cells contained substantial CPE that was characterized by massive apoptotic cell death with much expression of several endoplasmic reticulum (ER) stress-induced proteins [5]. Moreover, in HCV-JFH1 transfected Huh-7.5.1 cells, death occurred when all the cells were infected and the intracellular HCV RNA reached maximum levels [6]. Mishima *et al* further identified that mutant viruses with individual C2441S, P2938S, or R2985P signature substitutions enhanced virus replication and protein expression in the early/acute stages of infection, which finally led to massive cell death [7]. In addition, they also found that HCV-induced cytopathogenicity was closely associated with the level of intracellular viral replication and determined by certain amino acid substitutions in HCV-NS5A and -NS5B regions. Unfortunately, all of these studies were based on a recombinant virus model of liver cancer cells, and there are inevitable metabolic differences existing between hepatoma cell lines and quiescent primary hepatocytes. It is apparent that these cell lines cannot fully recapitulate all aspects of HCV infection in the liver, or the host responses playing important roles in determination of viral persistence or clearance [8]. In our previous study, we have established an infection system based on human fetal liver stem cells (hFLSCs) which could completely exhibit the entire blood-borne HCV (bbHCV) life cycle including transmission of the virus efficiently between cells. In the process of model building, we found that mitochondrial alterations and ER stress contribute a lot to our better understanding of HCV pathogenesis and provide insight

into the HCV life cycle. Therefore, we focused on using this cell model to investigate the effect of HCV infection on cells *in vitro*.

Materials and methods

Serum samples

HCV-positive serum samples were obtained from patients with chronic HCV infection treated at the Peking Union Medical College Hospital. Informed consent was obtained from all patients, and patients did not receive any antiviral therapy prior to this study. All donors had been serologically screened for syphilis, toxoplasmosis, rubella, hepatitis B, human immunodeficiency virus 1, cytomegalovirus, parvovirus, as well as herpes simplex types 1 and 2. Donor information is shown in supplementary material, Table S1.

hFLSCs infected by bbHCV and the progeny virus

hFLSCs were infected by bbHCV according to a previously described protocol [9]. In brief, sera or supernatant containing progeny virus were filtered through 0.22 μm polarized filters before infection. hFLSCs were grown to a 1×10^5 density in 6-well plates; and 2.4×10^6 genome copies (GCs)/ml of bbHCV or 2.3×10^6 GCs/ml of progeny virus with 1 ml of serum-free culture media were added into each well. After incubating for 8 h, cells were rinsed with DMEM/F_{12}. The final wash was collected and analyzed using RT-qPCR to confirm the absence of HCV RNA. Then, we added 1 ml of DMEM/F_{12} with 10% FBS for culturing. The supernatant was collected every other day during the culture period, and was stored at −80 °C. The detection and quantification of virus in hFLSCs or supernatant of infected cells were according to a previously described protocol [9].

Details of the protocol are presented in supplementary material, Supplementary materials and methods.

Electron microscopy observations

bbHCV- or mock-infected hFLSCs were fixed by incubation in 3% paraformaldehyde in 0.1 M PBS (pH 7.2) for 24 h. Cells were collected by centrifugation, the cell pellet was dehydrated in a graded series of ethanol solutions at −20 °C using an automatic freezing substitution system (AFS; Leica, Vienna, Austria), and embedded in London Resin Gold (LR Gold; Electron Microscopy Science, Basingstoke, UK). The resin was allowed to polymerize at −25 °C under UV light for 72 h. Ultra-thin sections were cut and blocked by incubation with 3% BSA (Sigma, St. Louis, MO, USA) in PBS; then, they were incubated with anti-E1 antibody as described above diluted at 1:50 in PBS supplemented with 1% BSA. Sections were washed and incubated with an appropriate volume of 10 nm gold particle-conjugated secondary antibody (British Biocell International, Cardiff, UK) diluted at 1:50 in PBS supplemented with 1% BSA. Ultra-thin sections were cut, stained with 5% uranyl acetate, 5% lead citrate, placed on EM grids coated with collodion, and examined.

Western blotting analyses

Proteins were prepared by using a Qproteome Mammalian Protein Prep Kit Column (Qiagen, Hilden, Germany). Total protein from cells and culture media were separated by 5–10% Bis-Tris sodium dodecyl sulfate-polyacrylamide gel electrophoresis (SDS-PAGE) and transferred to 0.45 μm PVDF membranes. Blots were blocked with 5% nonfat dry milk in Tris–HCl buffer saline (pH 7.5) containing 0.1% Tween-20 (TBST); and then, probed with primary antibodies for 1 h.

Western blotting was performed using the following antibodies: anti-HCV core (sc-81588, 1:500, Santa Cruz Biotechnology Inc., Dallas, TX, USA), anti-CHOP (sc-166682, 1:500, Santa Cruz Biotechnology Inc.), anti-GRP78 (sc-13539, 1:1000, Santa Cruz Biotechnology Inc.), anti-caspase-3 (sc-271759, 1:500, Santa Cruz Biotechnology Inc.), and anti-eIF2α proteins (sc-133227, 1:500, Santa Cruz Biotechnology Inc.), anti-IκB-α (W16166B, 1:600, Biolegend, San Diego, CA, USA), anti-IKK-β (2678, 1:2000, CST, Beverly, MA, USA), anti-NF-κB-p65 (8242, 1:1000, CST), anti-Bcl-xL (2762, 1:1000, CST), anti-XIAP (2042, 1:600, CST), anti-c-FLIPL (3210, 1:600, CST), anti-Akt (9272, 1:1000, CST), anti-PI-3K (4225, 1:1000, CST), and anti-JNK proteins (4668, 1:800, CST). After extensive washes, blots were incubated with secondary antibodies conjugated with horseradish peroxidase for 1 h then washed four times with TBST. Protein bands were detected using an enhanced chemiluminescence reagent and X-ray films.

Equal amounts of mitochondrial and cytosolic proteins (10 mg), prepared as previously described by Minczuk *et al* [10], were separated on 14% SDS–PAGE and then transferred to 0.22 μm PVDF membranes. For immunodetection, cytochrome *c* monoclonal antibody (556433, 1:1000, Pharmingen, San Diego, CA, USA) and actin polyclonal antibody (sc-70319, 1:5000, Santa Cruz Biotechnology Inc.) were used as primary antibodies. Mitochondrial fraction purity was verified by immunoblotting with antibodies specific to human cytochrome oxidase subunit II (COX II) (MA5-14568, 1:800, Molecular Probes, Waltham, MA, USA).

Flow cytometry

To measure HCV protein levels on the surface of hFLSCs, 5×10^5 cells were blocked with 1:50 BSA (Sigma) for 30 min prior to staining. Progression of primary and secondary antibody combinations was the same with the immunofluorescence process. Cells were stained with 4 μg/ml of propidium iodide in PBS before

being passed through a FACSCalibur flow cytometer (BD Biosciences, CA, USA). Mouse $IgG_1\kappa$–FITC (ab106163, 1:5000, Abcam, Cambridge, MA, USA) and rabbit $IgG_{2a}\kappa$–TRITC (ab18446, 1:5000, Abcam) were used as isotype controls. Experiments were repeated three times.

Bax activation analyses

To estimate the percentage of cells with activated Bax, bbHCV infected hFLSCs and control hFLSCs in the indicated time periods were incubated with rabbit polyclonal anti-Bax (sc-20067 1: 100, Santa Cruz Biotechnology Inc.) antibodies. Cells were then washed three times with PBS and stained with Texas Red conjugated-goat anti-rabbit IgG antibody (1:50). Finally, cells were washed three times with PBS and analyzed using a flow cytometer.

Oxidative stress analyses

To estimate production of ROS, bbHCV mock-infected and infected hFLSCs in the indicated time periods were exposed to MitoSOX Red, a fluorochrome specific to anion superoxide produced in the inner mitochondrial compartment (Invitrogen, Grand Island, NY, USA). Approximately 1×10^6 cells were trypsinized, incubated with MitoSox for 30 min at 37 °C, washed twice with PBS and resuspended in 500 µl of PBS and cytofluorometric analysis was performed using a flow cytometer.

ATP level measurement

The ATP level was examined by a firefly luciferase-based ATP assay kit (Beyotime, Haimen, China). The assay was conducted according to the manufacturer's instructions. In brief, after mitochondrial lysis, mitochondrial fractions were centrifuged at $10\,000 \times g$ for 10 min, and the supernatant was removed for the ATP assay. ATP reagents (100 µl) were added into a microwell for 5 min at 37 °C. The samples (50 µl) were then added and mixed for 10 s and measured using a Synergy HT multi-mode microplate reader. The ATP concentrations were calculated from standard curve data and expressed as nmol per mg protein.

Mitochondrial membrane potential ($\Delta\Psi m$) assessment

Mitochondrial membrane potential was determined by MitoProbe™ JC-1 Assay Kit for Flow Cytometry (Invitrogen) according to the manufacturer's instructions. In brief, 1×10^6 cells were suspended, incubated with 1 µl of 50 mM CCCP (control) or 10 µl of 200 µM JC-1 at 37 °C, 5% CO_2 for 15 min, and then washed once with 2 ml of warm PBS. Finally, the cells were resuspend by 500 µl PBS and analyzed by flow cytometer using 488 nm excitation.

Statistical analysis

All experiments were conducted in at least three separate experiments, and in duplicates. Data are expressed as mean ± SD, and was analyzed using SPSS for Windows version 17.0 (SPSS Inc., Chicago, IL, USA). P values < 0.05 were considered statistically significant.

Details for RT-qPCR assays, serum characteristics, primers and probes sequences are presented in supplementary material, Supplementary materials and methods.

Results

bbHCV induced cytopathogenicity in hFLSCs

We assessed electron microscopic images to determine whether a CPE existed in bbHCV-infected hFLSCs. In contrast to control sections where the ER was linear and the typical cytoplasmic distribution of mitochondria with intact cristae was observed (Figure 1A), cell sections infected by bbHCV had ER distention and mitochondrial swelling (Figure 1B,C and supplementary material, Figure S1A). Numerous double membrane vesicles (DMVs) and the presence of more discrete multivesicular units had features similar to those that were observed in other RNA viruses such as poliovirus and coronavirus (Figure 1D and supplementary material, Figure S1B). However, this effect could not be observed in cells exposed to UV-inactivated bbHCV (see supplementary material, Figure S1C,D), which indicated that these phenomena were definitively caused by active viral replication.

bbHCV infection sensitizes cells to cellular apoptosis

The majority of hFLSCs infected with bbHCV did not eventually show cell death. When the cells were stained with DAPI for nuclear morphology at various times postinfection, only cells with bbHCV infection at 16 h postinfection revealed nuclear shrinkage, a feature of cellular apoptosis (Figure 2A). In order to further assess whether infected cells were involved in an apoptotic process, we performed annexin V staining with flow cytometry analysis; and found that the levels of annexin V positivity increased with the extending of time and reached a peak of 29.8% within hFLSC at 16 h postinfection, and then declined after 48 h postinfection (Figure 2B,C and supplementary material, Figure S2).

ER stress-related proteins in hFLSCs following bbHCV infection

We then explored the role ER stress plays in cells apoptosis. The expression of ER stress-related proteins, GRP78 and phosphorylated eIF2-alpha were assessed in bbHCV-infected cells. The overexpression of GRP78 and phosphorylated eIF2-alpha strongly suggested that bbHCV infection could induce ER stress as an early cell

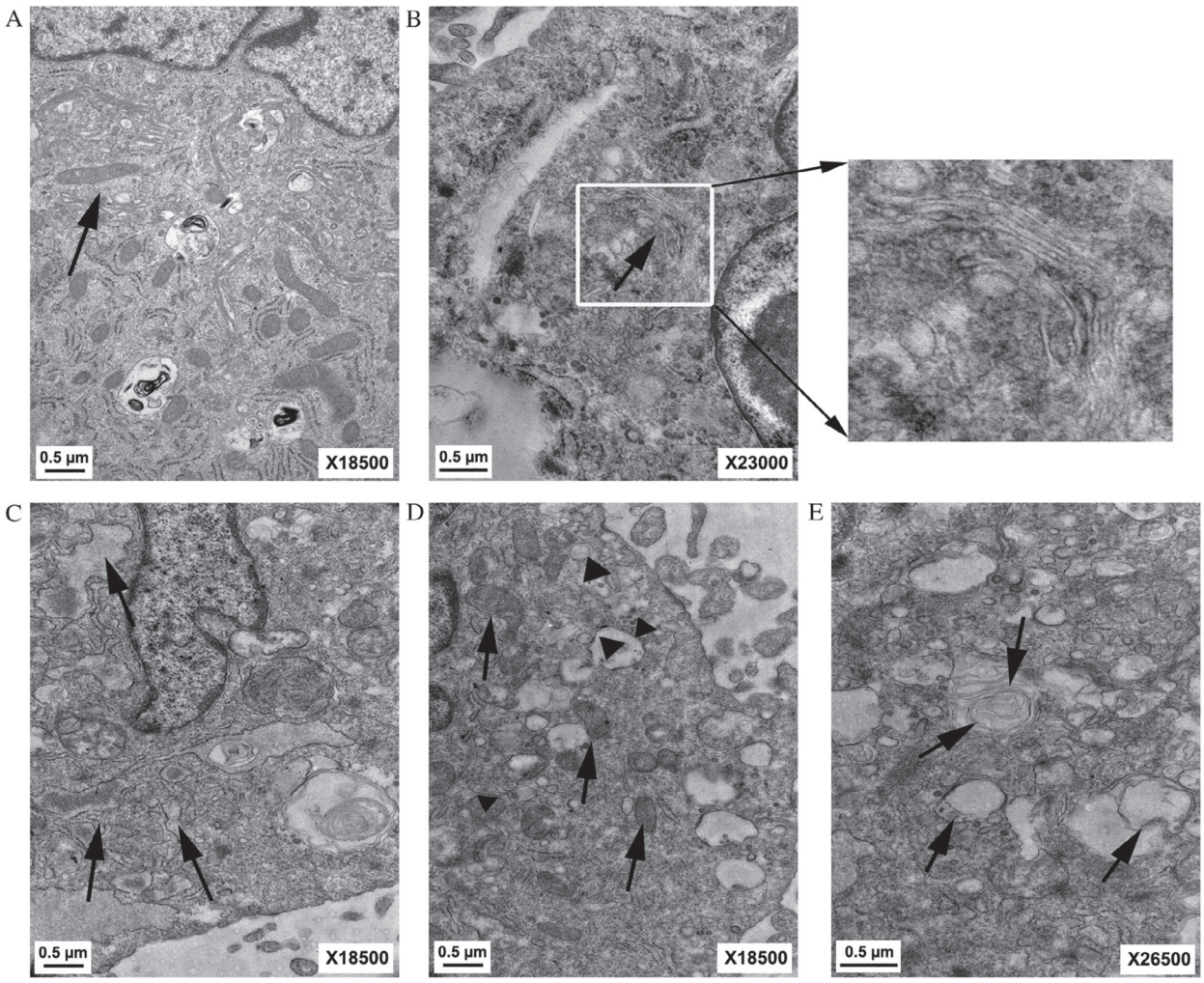

Figure 1. bbHCV induced cytopathogenicity in hFLSCs. (A and B) Normal ER and mitochondria of hFLSCs in control sections (arrows). (C–E) bbHCV-infected hFLSCs sections revealed: (C) convolution and nonliner ER (arrows), (D) cell vacuolization (arrowheads), swelling mitochondria (arrows), (E) numerous DMVs (arrows).

response (Figure 3). Persistence of ER stress activated apoptosis signaling pathways, including the induction of C/EBP homologous protein (CHOP) and the activation of caspase 3 (Figure 3) closely related with cell death. Similar to annexin V, these proteins peaked at 16 h or 24 h postinfection and declined at 48 h postinfection.

It has been reported that CHOP overexpression may lead to Bax activation and translocation from the cytosol to mitochondria [11]. We found that Bax activation and clustering to mitochondria occurred in 20% of bbHCV infected cells at 16 h postinfection (Figure 4A), but decreased after 24 h postinfection. It is well known that Bax activation could induce mitochondrial membrane depolarization [12]. We then investigated the effect of bbHCV infection on mitochondrial membrane potential ($\Delta\Psi m$). The proportion of cells with decreased $\Delta\Psi m$ in bbHCV-infected cells is much higher than that in controls (Figure 4B and supplementary material, Figure S3). Meanwhile, levels of mitochondrial ROS and intracellular ATP displayed similar results as $\Delta\Psi m$ (Figure 4C,D).

Cytochrome c associated with HCV replication could be released into the cytosol in bbHCV-infected cells (Figure 5A). Finally, we sought to determine whether HCV could lead to the activation of terminal caspases by using anti-caspase-3 antibody which could recognize both the procaspase and the cleaved active caspase 3 p11 subunit. We found the p11 cleaved active subunit of the caspase-3 at 16 h postinfection (Figure 5B). These results demonstrated that bbHCV infection could definitively induce an advanced apoptotic process at the early stage of infection.

bbHCV infection activates anti-apoptotic proteins

Apoptosis proteins were decreased at 24 h postinfection. The majority of cells recovered and did not show apparent death afterwards. The expression of NF-κB dependent anti-apoptotic proteins and phosphorylation status of AKT in infected hFLSCs were investigated. Immunoblotting analysis revealed that the expressions of the well-known anti-apoptotic proteins, NF-κB-p65, Bcl-xL and XIAP, and the long form of cFLIP (c-FLIPL) [13], were markedly activated in bbHCV-infected cells after 24 h post infection (Figure 5C,D). Meanwhile, Ser^{473} phosphorylation of AKT increased in bbHCV

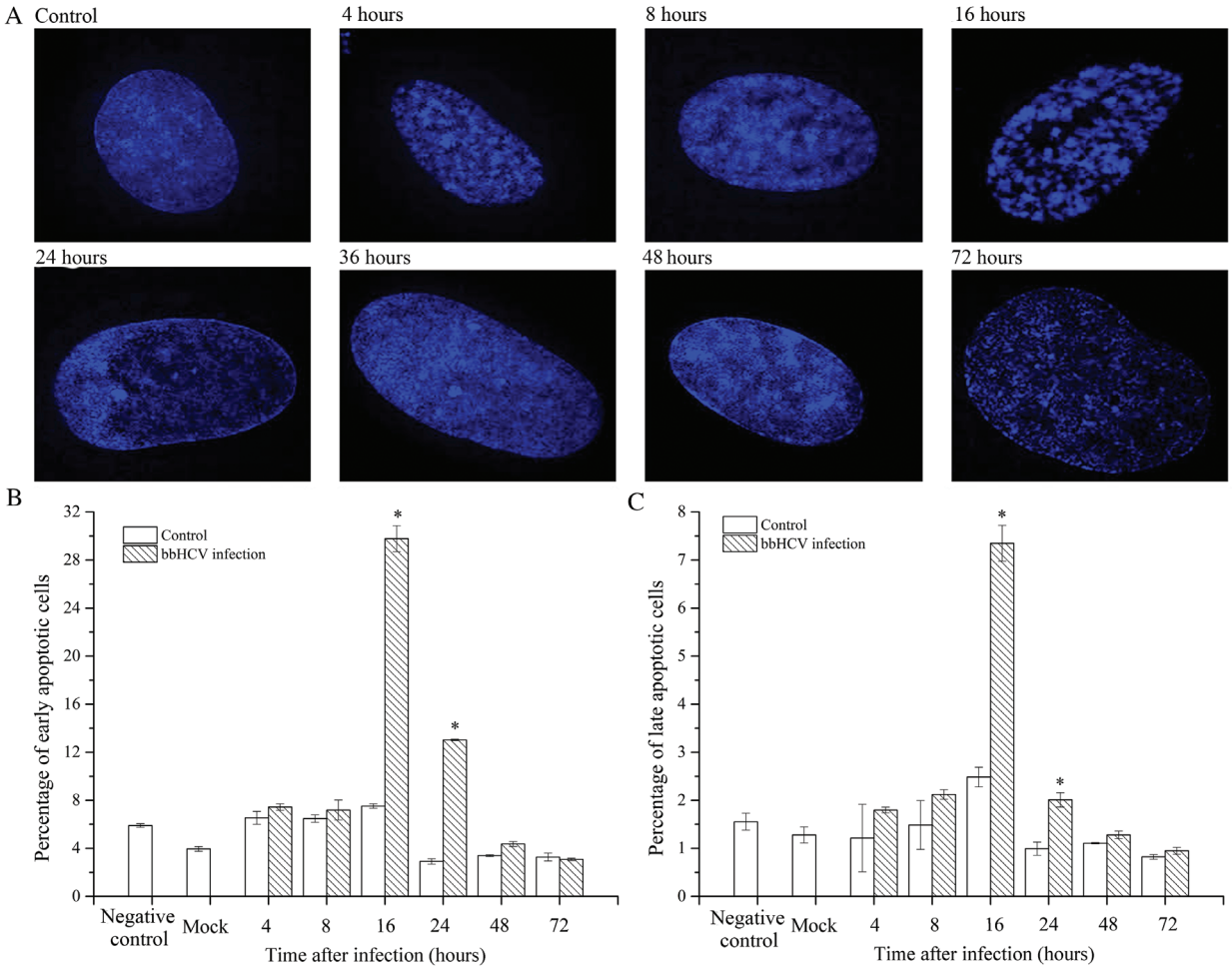

Figure 2. HCV infection caused hFLSCs apoptosis. (A) hFLSCs were infected with or without bbHCV for different times as indicated. The cells were harvested and stained with DAPI. The scale bar represents 5 μm. (B and C) Kinetics of apoptosis in bHCV-infected hFLSCs was determined with annexin V expression. hFLSCs were harvested at indicated times after infection for annexin V expression by flow cytometric analysis. The percentage of early and late apoptotic cells was plotted. The results shown are representative of three independent experiments done in triplicates. Error bars represent the mean ± SD. $^*p < 0.05$ versus control.

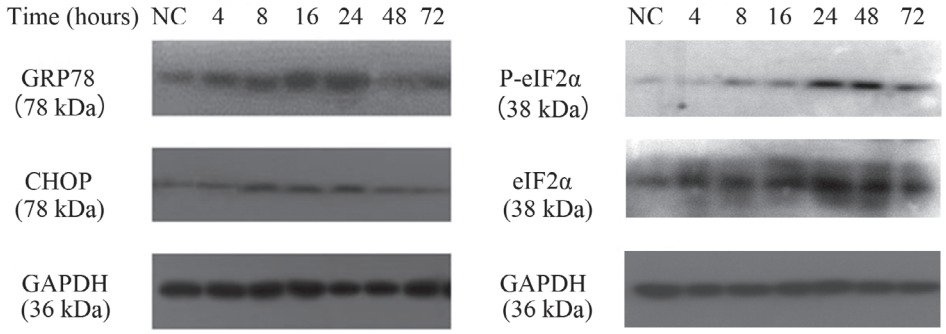

Figure 3. The expression of ER stress-related proteins in bbHCV infected cells. Western blotting was performed using anti-GRP78, anti-p-eIF2α, anti-eIF2-α, anti-CHOP, and anti-GAPDH.

infected cells, whereas Thr^{308} phosphorylation levels were not significantly altered after infection with bbHCV (Figure 5E). Simultaneously, increased expression of *TYMS*, *JUND*, and *UBD* mRNAs, whose protein functions relate to the decrease of p53 levels and the supply of a protective effect against p53-dependent apoptosis, suggested that the cell counteracted the activation of the p53 signaling pathway (Figure 5F).

Discussion

HCV infection induced CPE is part of the infection process. Whether the established infection model could simulate and undergo CPE similar to lesions observed in hepatitis patients could be a measure of the model's success. The presentation of HCV-induced CPE is vital in cell culture systems, and could contribute to the

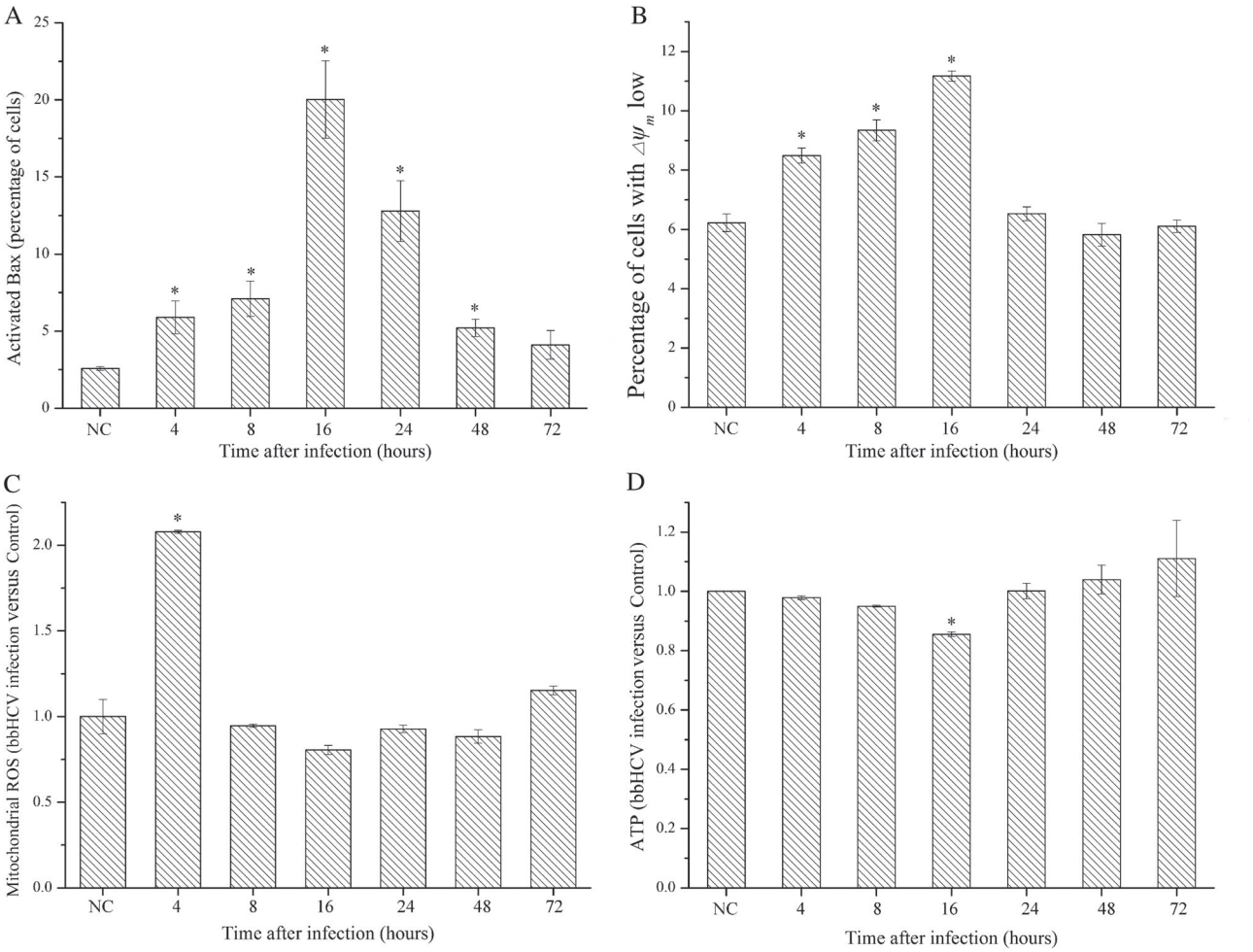

Figure 4. bbHCV infection induced mitochondrial stress in hFLSCs. (A) Bax activation after bbHCV infection at indicated times was analyzed by flow cytometry, and data were presented as percentage of cells with activated Bax clustering within mitochondria. (B) bbHCV infection induced a decrease in mitochondrial membrane potential ($\Delta\Psi m$) in hFLSCs, and data were presented as percentage of cells with decreased in $\Delta\Psi m$. (C) Assessment of superoxide generation in bbHCV infected hFLSCs and control in the indicated time periods by MitoSOX Red. (D) ATP synthesis in in bbHCV infected hFLSCs and control hFLSCs. The results are representative of three independent experiments. Error bars represent the mean ± SD. *$p < 0.05$ versus control.

understanding of HCV pathogenesis. In our system, CPEs induced by bbHCV infection including ER distention, mitochondrial swelling and cell vacuolization were similar to cell lesions derived from chronic HCV patients. The mechanisms of the pathogenesis induced by bbHCV infection might be traced back to ER-stress and mitochondria-related/caspase-dependent apoptosis in hFLSCs at the early stages of infection. With time going on, apoptosis would gradually be inhibited by the increasing expression of bcl-XL, the activation of NF-κB, the survival pathway of PI3-kinase-AKT/PKB, and the sequestering of p53. NF-κB activation disrupts the balance between the survival cells and the infected cells by inhibiting apoptosis. The accelerated cycles of cell apoptosis, regeneration and repair resulting from HCV infection could shorten the cell death cycle and give rise to the development of cirrhosis, and ultimately lead to hepatocellular carcinogenesis.

It has been reported that the PI3K/AKT and/or NF-κB signaling pathways could lead to upregulation of HIF-1α [14]. Then, the HIF-1α subunit being located in nuclei could cause inhibition of respiratory activity, with depression of the mitochondrial complex I along with uncoupling of mitochondrial oxidative phosphorylation efficiency [15]. Our data also provided a strong demonstration that ATP production increased in cells infected by bbHCV. An over-compensatory glycolytic metabolic response might be responsible for the phenomenon above by impairing mitochondrial oxidative phosphorylation efficiency. In addition, bbHCV-induced mitochondrial oxidative phosphorylation impairment is associated with oxidative stress that clearly tracks to the mitochondrial compartment where the ROS O^{2-} is first formed; then the ROS O^{2-} triggers the permeability transition pore through which cytochrome *c* could be released and diffuse into the cytosol. Ultimately, the cytochrome *c* would induce the apoptotic program and cause subsequent cell damage.

It has been reported that hepatocytes are injured in HCV-infected patients. High serum HCV levels pre- and postliver transplant were associated with cholestatic

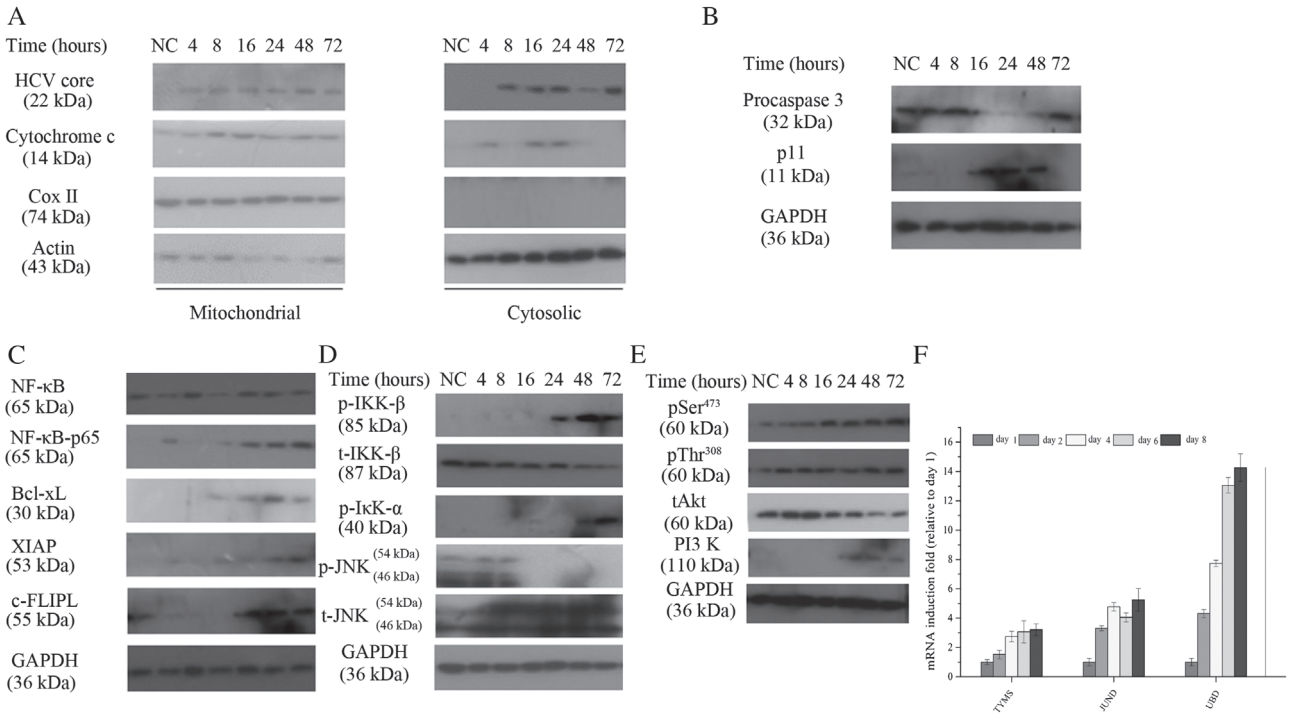

Figure 5. (A) Mitochondrial and cytosolic fractions prepared from hFLSCs mock-infected or infected with bbHCV were analyzed by western blotting using anti-cytochrome *c*, anti-COXII (reference of mitochondrial fraction purity), anti-actin and anti-HCV core. Western blotting analysis with anti-cytochrome c antibody revealed an increased amount of cytochrome c in the cytosolic protein fraction of bbHCV-infected hFLSC compared to control. (B) bbHCV infection activates caspase 3. Western blotting analysis was performed using anti-caspase-3 after hFLSCs mock-infected or infected with bbHCV at the indicated times. (C) bbHCV infection induced NF-κB activation in hFLSCs after 24 h, the expression of NF-κB-p65, Bcl-xL, XIAP, and c-FLIPL were evaluated by western blotting in hFLSCs with or without bbHCV infection. (D and E) bbHCV infection induced activation of NF-κB and the PI3-kinase-Akt/PKB survival pathway as well as sequestering of p53. bbHCV infected or noninfected hFLSCs were cultured for various periods (0–72 h). Cell lysates were subjected to immunoblotting analyses of (D) IKK, IκB, and JNK and (E) AKT and PI3 K. GAPDH was used as a loading control. (F) Induction of genes (*TYMS*, *JUND*, and *UBD*) encoding proteins which function to either decrease p53 levels or serve as a protective effect against p53-dependent apoptosis in hFLSCs with or without bbHCV infection were measured by RT-qPCR and normalized against *GAPDH*. The results were the fold induction relative to day 1. The results are representative of three independent experiments. Error bars represent the mean ± SD. NC, negative control.

fibrosis, a severe form of hepatitis [16]. EM of HCV RNA-positive liver biopsies showed that the hepatocytes would undergo vacuolation and lysis of membrane organelles, degeneration of mitochondria, dilatation of cytoplasmic reticulum tubules, and formation of an appreciable amount of large polymorphic secondary phagosomes [17]. Kasprzak *et al* summed up the data on nuclear lesions of liver biopsies with chronic HCV infection, involving swelling, altered shape, hyperchromasia, disturbed nuclear chromatin structure; and the nuclear lesions always occurred in the cells with changes in rough ER within long tubular structures or branching fibrils inside [18]. Other cytoplasmic changes included mitochondrial lesions, numerous lipid vacuoles and free tubular structure of a highly osmiophilic character [18]. Similarly, Falcón *et al* studied liver biopsies from patients with chronic HCV infection [19]. They found that all liver biopsy samples from these 13 chronically HCV-infected patients showed ultrastructural cell damage. Ballooning hepatocytes with dilatation of the ER and mitochondria were observed. More importantly, studies have shown that fibrosis progress was more vulnerable in coinfected patients with HIV than that in monoinfected patients, leading to the increasing rates of cirrhosis and complications [20,21]. The loss of secondary immunity against HCV could provide a possible explanation for the higher persistence rate of HCV in the coinfection patients with HIV, and histologic variants in liver biopsy specimens of coinfected individuals might be due to the direct cytopathic activity of HCV [22]. In contrast, Seong-Jun *et al* conducted EM to observe Huh7 cells harboring HCV full length replicon (JFH1), which revealed prominent clustering of mitochondria in the perinuclear regions within HCV infected cells and a dramatic loss of mitochondrial cristae compared with the uninfected cells [23]. Katze *et al* attempted to gain insight into the mechanisms of HCV-associated cell death by performing microarray experiments on Huh-7.5 cells infected with HCV-J6/JFH [24]. The presence of activated caspase-3 and cell death-related genes both strongly indicated that HCV infection was associated with a direct CPE. A wealth of published literature has referred to some experiments in which one or more HCV proteins could induce cytopathogenicity in cultured hepatocytes. Core protein has been reported to have both pro- and anti-apoptotic effects on death ligand mediated hepatocyte apoptosis [25,26]. The HCV envelope protein

E2 has been found to inhibit TRAIL-induced apoptosis and induce mitochondria-related/caspase-dependent apoptosis in hepatoma cell line [27]. Perturbations of apoptotic pathways have also been demonstrated with the nonstructural proteins [28–31].

The above situation suggested that HCV could induce cell damage *in vivo* and *in vitro*. And the main CPEs described previously were similar to those we observed in bbHCV infected hFLSCs including ER distention, mitochondrial swelling and cell vacuolization. This model is expected to provide a more powerful tool for studying the cytological mechanisms of HCV infection *in vitro* and exploring the development of cirrhosis and hepatocellular carcinogenesis.

Acknowledgements

We would like to thank the National Institute for Viral Disease Control and Prevention and the Chinese Center for Disease Control and Prevention for our electron microscopy work (and we are grateful to JDS for his technical assistance of taking and analyzing electron microscopy images of virus in culture media and hFLSCs). This work was supported by the Youth Talent Support Project of China Association for Science and Technology (Grant No. 17-JCJQ-QT-019).

Author contributions statement

All authors contributed to this article. XG completed the main experiments and drafted the full manuscript. DY and WLL completed part of the trials for HCV detection. ZQS and ZGQ completed the partial experiments in the process of the revised manuscript. JWL and MJ conceived and designed the experiments and contributed to editing the manuscript.

References

1. Abdelwahab SF. Cellular immune response to hepatitis-C-virus in subjects without viremia or seroconversion: is it important? *Infect Agent Cancer* 2016; **11:** 23.
2. Lechmann M, Ihlenfeldt HG, Braunschweiger I, *et al.* T- and B-cell responses to different hepatitis C virus antigens in patients with chronic hepatitis C infection and in healthy anti- hepatitis C virus-positive blood donors without viremi. *Hepatology* 2010; **24:** 790–795.
3. Mengshol JA, Goldenmason L, Rosen HR. Mechanisms of disease: HCV-induced liver injury. *Nat Clin Pract Gastroenterol Hepatol* 2007; **4:** 622–634.
4. Ivanov AV, Bartosch B, Smirnova OA, *et al.* HCV and oxidative stress in the liver. *Viruses* 2013; **5:** 439–469.
5. Sekine-Osajima Y, Sakamoto N, Mishima K, *et al.* Development of plaque assays for hepatitis C virus-JFH1 strain and isolation of mutants with enhanced cytopathogenicity and replication capacity. *Virology* 2008; **371:** 71–85.
6. Zhong J, Gastaminza P, Chung J, *et al.* Persistent hepatitis C virus infection in vitro: coevolution of virus and host. *J Clin Virol* 2006; **36:** S21–S21.
7. Mishima K, Sakamoto N, Sekine-Osajima Y, *et al.* Cell culture and in vivo analyses of cytopathic hepatitis C virus mutants. *Virology* 2010; **405:** 361–369.
8. Bartenschlager R, Pietschmann T. Efficient hepatitis C virus cell culture system: what a difference the host cell makes. *Proc Natl Acad Sci U S A* 2005; **102:** 9739–9740.
9. Guo X, Wang S, Qiu Z-G, *et al.* Efficient replication of blood-borne hepatitis C virus in human fetal liver stem cells. *Hepatology* 2017; **66:** 1045–1057.
10. Minczuk M, Piwowarski J, Papworth MA, *et al.* Localisation of the human hSuv3p helicase in the mitochondrial matrix and its preferential unwinding of dsDNA. *Nucleic Acids Res* 2002; **30:** 5074–5086.
11. Jiang X, Jiang H, Shen Z, *et al.* Activation of mitochondrial protease OMA1 by Bax and Bak promotes cytochrome c release during apoptosis. *Proc Natl Acad Sci U S A* 2014; **111:** 14782–14787.
12. Szlosarek PW, Klabatsa A, Pallaska A, *et al.* Arginine depletion upregulates Bax and triggers apoptosis of malignant mesothelioma cells deficient in argininosuccinate synthetase. *Cancer Res* 2006; **66:** 521.
13. Lee SH, Song R, Lee MN, *et al.* A molecular chaperone glucose-regulated protein 94 blocks apoptosis induced by virus infection. *Hepatology* 2008; **47:** 854–866.
14. Van UP, Kenneth NS, Rocha S. Regulation of hypoxia-inducible factor-1alpha by NF-kappaB. *Biochem J* 2008; **412:** 477–484.
15. Claudia P, Rosella S, Giovanni Q, *et al.* Hepatitis C virus protein expression causes calcium-mediated mitochondrial bioenergetic dysfunction and nitro-oxidative stress. *Hepatology* 2010; **46:** 58–65.
16. Doughty AL, Spencer JD, Cossart YE, *et al.* Cholestatic hepatitis after liver transplantation is associated with persistently high serum hepatitis C virus RNA levels. *Liver Transpl Surg* 1998; **4:** 15–21.
17. Postnikova OA, Aidagulova SV, Nepomnyashchikh DL, *et al.* Ultrastructural and stereological study of the liver in chronic mixed HCV + HBV infection. *Bull Exp Biol Med* 2012; **152:** 764–767.
18. Kasprzak A, Biczysko W, Adamek A, *et al.* Morphological lesions detected by light and electron microscopies in chronic type C hepatitis. *Pol J Pathol* 2003; **54:** 129–142.
19. Falcon V, Acosta-Rivero N, Chinea G, *et al.* Ultrastructural evidences of HCV infection in hepatocytes of chronically HCV-infected patients. *Biochem Biophys Res Commun* 2003; **305:** 1085–1090.
20. Graham CS, Baden LR, Yu E, *et al.* Influence of human immunodeficiency virus infection on the course of hepatitis C virus infection: a meta-analysis. *Clin Infect Dis* 2001; **33:** 562–569.
21. Benhamou Y, Bochet M, Di Martino V, *et al.* Liver fibrosis progression in human immunodeficiency virus and hepatitis C virus coinfected patients. The Multivirc Group. *Hepatology* 1999; **30:** 1054–1058.
22. Rosenberg PM, Farrell JJ, Abraczinskas DR, *et al.* Rapidly progressive fibrosing cholestatic hepatitis–hepatitis C virus in HIV coinfection. *Am J Gastroenterol* 2002; **97:** 478–483.
23. Kim SJ, Syed GH, Siddiqui A. Hepatitis C virus induces the mitochondrial translocation of Parkin and subsequent mitophagy. *PLoS Pathog* 2013; **9:** e1003285.
24. Walters KA, Syder AJ, Lederer SL, *et al.* Genomic analysis reveals a potential role for cell cycle perturbation in HCV-mediated apoptosis of cultured hepatocytes. *PLoS Pathog* 2009; **5:** e1000269.
25. Lai MM, Ware CF. Hepatitis C virus core protein: possible roles in viral pathogenesis. *Curr Topic Microbiol Immunol* 2000; **242:** 117–134.
26. Saito K, Meyer K, Warner R, *et al.* Hepatitis C virus core protein inhibits tumor necrosis factor alpha-mediated apoptosis by a protective effect involving cellular FLICE inhibitory protein. *J Virol* 2006; **80:** 4372–4379.
27. Lee SH, Kim YK, Kim CS, *et al.* E2 of hepatitis C virus inhibits apoptosis. *J Immunol* 2005; **175:** 8226–8235.

28. Prikhod'ko EA, Prikhod'ko GG, Siegel RM, *et al.* The NS3 protein of hepatitis C virus induces caspase-8-mediated apoptosis independent of its protease or helicase activities. *Virology* 2004; **329:** 53–67.
29. Lan KH, Sheu ML, Hwang SJ, *et al.* HCV NS5A interacts with p53 and inhibits p53-mediated apoptosis. *Oncogene* 2002; **21:** 4801–4811.
30. Chung YL, Sheu ML, Yen SH. Hepatitis C virus NS5A as a potential viral Bcl-2 homologue interacts with Bax and inhibits apoptosis in hepatocellular carcinoma. *Int J Cancer* 2003; **107:** 65–73.
31. Sarcar B, Ghosh AK, Steele R, *et al.* Hepatitis C virus NS5A mediated STAT3 activation requires co-operation of Jak1 kinase. *Virology* 2004; **322:** 51–60.

SUPPLEMENTARY MATERIAL ONLINE

Supplementary materials and methods

Supplementary figure legends

Figure S1. bbHCV induced cytopathogenicity in hFLSCs

Figure S2. hFLSCs infected or mock-infected by bbHCV were harvested at the indicated times for annexin V expression by flow cytometric analysis

Figure S3. hFLSCs infected or mock-infected by bbHCV were harvested at the indicated times for JC-1 by flow cytometric analysis

Table S1. Serum characteristics and RNA quantity after infecting hFLSCs

Table S2. Primers and probes used in this study